



# Experimental investigation of influence of alternating cyclic loadings on creep behaviors of sandstone

Chongfeng Chen<sup>1,2</sup> · Tao Xu<sup>1</sup>  · Guanglei Zhou<sup>1</sup> ·  
Tao Qin<sup>3</sup>

Received: 21 January 2019 / Accepted: 4 November 2019 / Published online: 21 November 2019  
© Springer Nature B.V. 2019

**Abstract** Cyclic stress variation induced by mining activities has a significant effect on the stability of surrounding rock and mining pillar in deep underground engineering. The influence of alternating cyclic loading and unloading tests on creep behavior of sandstone was investigated to explore the mechanism of the effect of the cyclic stress variation on the stability of rock. Firstly, a series of uniaxial constant strain rate and multi-step monotonic creep tests of sandstone were carried out to determine the maximum high loading stress and the minimum low loading stress in the alternating cyclic creep tests. Then the alternating cyclic loading and unloading creep tests were conducted to investigate the effects of loading paths and loading histories of cyclic high stress creep and low stress creep on the creep behavior of sandstone. Acoustic emission events, axial strain rate and lateral strain rate were also analyzed. The experimental results show that loading paths and loading histories of high stress creep and low stress creep have a significant influence on the alternating cyclic creep behavior of sandstone. The loading paths could accelerate the damage in the rock sample, which can be demonstrated by much larger plastic strain occurring in the damaged sample and larger viscous strain in the creep behavior of less damaged sample. The loading histories could increase viscous strain and plastic strain in the damaged sample. The maximum and the minimum loading stresses determined by the unstable crack threshold provide the basis of the unstable cracks growth in rock sample. The work presented in the present paper is helpful to understand the mechanical behaviors of rock mass under cyclic underground mining activities.

**Keywords** Creep behavior · Damage cracks · Volumetric compaction · Volumetric dilatancy · Alternating cyclic creep tests

---

✉ T. Xu  
[xutao@mail.neu.edu.cn](mailto:xutao@mail.neu.edu.cn)

<sup>1</sup> Center for Rock Instability & Seismicity Research, Northeastern University, Shenyang 110819, China

<sup>2</sup> Xi'an Research Institute, China Coal Technology and Engineering Group, Xi'an 710054, China

<sup>3</sup> Heilongjiang Ground Pressure and Gas Control in Deep Mining Key Lab, Heilongjiang University of Science and Technology, Harbin 150027, China

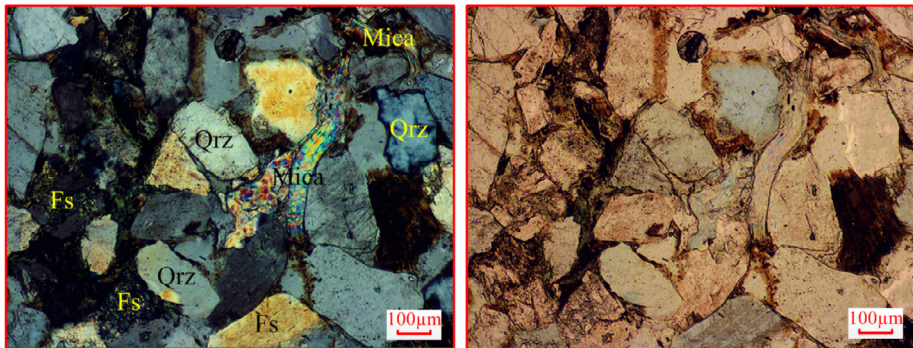
## 1 Introduction

Brittle rocks can deform and fail under constant applied stresses that are well below their short-term failure strength over extended periods of time. Such time-dependent deformation of brittle rock at constant stress is termed as brittle creep, a process leading to delayed failure (Brantut et al. 2013; Challamel et al. 2006; Kranz et al. 1982; Liu et al. 2017; Xu et al. 2012; Zhou et al. 2013). A detailed knowledge of brittle creep of rock is a vital prerequisite for understanding the long-term behavior of the rocks within the upper crust of the Earth. The comprehension of rock creep behavior is not only crucial for assessing geophysical hazards such as earthquake ruptures and volcanic eruptions (Bell et al. 2011; Lyakhovsky and Ben-Zion 2008), but also for the construction and long-term stability of engineering structures such as underground mines and excavations (Brouard et al. 2013; Zhang et al. 2016b), nuclear waste storage facilities (Yang and Edwards 2000), and tunnels (Jeng et al. 2002).

Underground engineering accidents induced by mining or excavation, such as rockburst, roof falling, and even mine collapse, have frequently caused a great loss to the community (Chen et al. 2012). Most of the accidents are closely related to the change of in situ stress, especially alternating cyclic loading and unloading on the surrounding rock or mining pillar (Fairhurst 2003; Szwedzicki 2003). The stress variation induced by the mining activities, such as coal cutting, tunnel excavation and support, destress blasting, and longwall mining plays a significant role in the stability of the surrounding rock or the mining pillar (Brady and Brown 2013; Kaiser and Cai 2012; Konicek 2018; Konicek et al. 2013; Li et al. 2017; Petr et al. 2011). Furthermore, rock mass at great depths experiences creep deformation all the time (Armand et al. 2013; Atsushi and Mitri 2017). Once the rock mass is disturbed by mining activities in the deep underground, it may easily fail during underground mining or excavation activities (Li et al. 2012; Mazaira and Konicek 2015).

At present, extensive experimental work devoted to different aspects of creep has been undertaken. Most of creep tests focus on the influence of environmental conditions such as differential stress (Wang et al. 2015; Zhang et al. 2016b), confining pressure (Wang et al. 2014; Xu et al. 2018), fluid pressure (Heap et al. 2009b; Jeong et al. 2007), temperature (Heap et al. 2009a; Niemeijer et al. 2002; Xu et al. 2017) and microstructural state (Brantut et al. 2013; Eslami et al. 2012) on the time-to-failure and/or the creep strain rate. For example, Heap has made great efforts in performing tri-axial creep tests on Darley Dale sandstone and basalt in order to observe the initiation or precursors of accelerating creep and to clarify the rock damage and failure mechanism associated with accelerating creep (Heap et al. 2009b, 2011). Although an extensive effort has been made to investigate the influence of environmental conditions on creep mechanical properties of rock, little work on the effect of complex loading stress paths on creep behavior of rock has been performed to date.

Based on the understanding of fatigue tests (Cerfontaine and Collin 2018), some researchers have paid attention to the influence of unloading and loading cycles on the creep behavior of rock. Fabre and Pellet (2006) focused on the creep tests coupling with unloading and loading cycles, and found that a cyclic load can accelerate the development of viscoplastic deformation and, therefore, reduce the test duration. Sone and Zoback conducted multi-step creep experiments coupling with unloading and reloading cycle in the applied axial differential load to study the ductile creep properties and the brittle strengths properties of shale-gas reservoir rocks (Sone and Zoback 2013a, 2013b, 2014). They found that the time-dependent deformation exhibits hysteretic behavior when samples undergo unloading/reloading stresses, and the strain recovery upon unloading of stress appears to



(a) Photomicrograph under cross-polarized light (b) Photomicrograph under plane-polarized light.

**Fig. 1** Photomicrograph of sandstone (Chen et al. 2018b)

be slower compared to the creep strain rate upon loading. Recently, Yanlin Zhao analyzed the instantaneous elastic strain, visco-elastic strain, instantaneous plastic strain and visco-plastic strain in the creep tests conducted on the soft rock under multi-level loading and unloading cycles, and finally proposed a nonlinear elasto-visco-plastic rheological model (Zhao et al. 2009, 2017a, 2017b). Shengqi Yang also used the same method as Zhao et al. (2017a) on red sandstones to analyze the elastic, visco and plastic strain and established a nonlinear elastic-visco-plastic rheological damage model (Hu et al. 2018; Yang and Hu 2018). Furthermore, Chen et al. (2018a) carried out some uniaxial experiments to reveal the influence of unloading and loading stress cycles on the creep behavior, and they found that the procedure of unloading and loading the stress during a constant stress creep test transiently increases the strain and AE hit rate. Though there are already a lot of work about creep tests coupling with unloading and loading cycles, the work about the effect of cyclic unloading and loading stresses on the creep behavior and considering the influence of loading paths, alternating maximum loading stress and minimum loading stress, is still lacking.

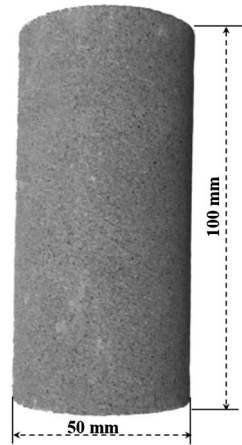
In the present study, we first perform uniaxial compressive strength tests to get uniaxial strength parameters of sandstone. Based on the result of constant strain rate tests, uniaxial multi-step creep tests are performed to determine the appropriate high and low loading stresses used in cyclic creep and alternating cyclic testing. Finally, some multistage cyclic creep experiments, coupling creep and alternating cyclic tests, are performed on sandstone to investigate the effects of stress histories of high stress creep and low stress creep on multistep cyclic creep, and we attempt to uncover the underlying mechanisms for the transition from fatigue to creep in rock under multistage cyclic creep experiments. Our hope is that some results of this paper could provide help in understanding mechanical mechanisms in rock engineering problems.

## 2 Materials and methods

### 2.1 Sample material and preparation

The sandstone used throughout this study was collected from a quarry in the city of Neijiang, Sichuan Province, China (Chen et al. 2018b). The sandstone is a well-indurated, feldspathic

**Fig. 2** Rock specimens used in the study; No distinct layering or lamination is shown



sandstone whose composition is 60% quartz, 20% feldspar, 15% cement and 5% mica, and whose porosity is  $4.5 \pm 0.5\%$  (Wang et al. 2016). Optical microscopy analyses demonstrated that the grains are sub-angular, varying in size from 200–500  $\mu\text{m}$  (Fig. 1). All samples were cored from the same sandstone block to a diameter of  $50 \pm 0.02$  mm. They were precision-ground to  $100 \pm 0.02$  mm in length, resulting in a length: diameter ratio of 2:1. The sandstone sample produced from the blocks is shown in Fig. 2. No distinct layering or lamination could be observed in samples by naked-eye. The P-wave velocity is about  $1.77 \text{ km s}^{-1}$  for natural samples of sandstone, and the variation of P-wave velocity for all samples used in the present research is within  $\pm 0.05 \text{ km s}^{-1}$  to decrease the sample difference.

## 2.2 Experimental methodology

All specimens were tested at room temperature on a servo-controlled TOP INDUSTRIE tri-axial testing machine as shown in Fig. 3a. The maximum load capacity of axial compression is 720 kN and the cell is designed to resist a confining pressure of 60 MPa. The sample can be mounted with both axial and lateral measurement devices simultaneously. Four linear variable differential transformer (LVDT) axial displacement transducers measure axial deformation; and four LVDT lateral displacement transducers measure lateral deformation (Fig. 3b). Volumetric strain was calculated by the summation of both axial and double lateral strains (or circumferential strain) (Li et al. 2018). Samples were mounted between two steel end-caps, and some petrolatum was imbedded between samples and steel end-caps to reduce the end effect. Acoustic emission (AE) output was recorded continuously by eight acoustic emission (AE) transducers mounted on the sample using elastic rubber ring (as shown in Fig. 3b).

Considering the variation of mechanical behaviors of samples even from the same rock block, multi-step creep tests on one sample were adopted to avoid the sample variation. In the present study, two types of alternating cyclic unloading and loading creep tests, i.e., low-high-low (simplified by LHL in the following) stress sequence and high-low-high (HLH) stress sequence, were conducted to study the effect of loading history on creep behaviors of sandstone. Prior to performing creep tests, a series of uniaxial compressive tests at a constant strain rate of  $1.0 \times 10^{-5} \text{ s}^{-1}$  were firstly conducted on sandstone to obtain the short-term deformation and failure characteristics of sandstone. Uniaxial compressive strength, Young's

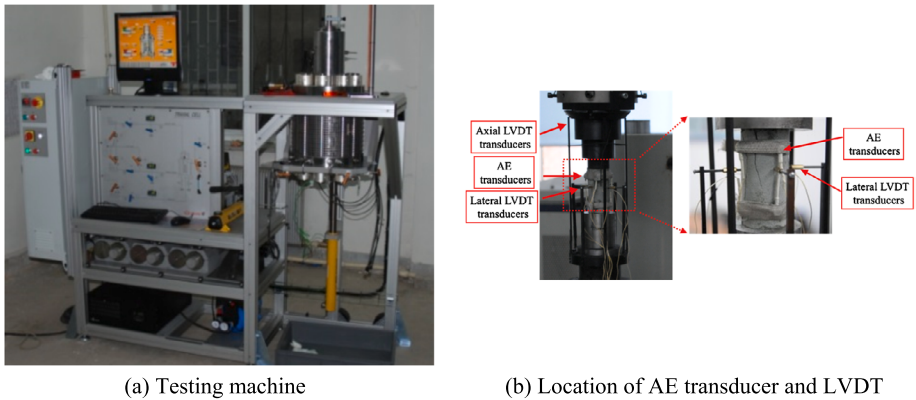


**Fig. 3** Servo-controlled rock rheology testing machine

**Table 1** Stress loading sequences for multi-step monotonic creep tests

Stages	Stress (MPa)	Ratio of UCS (%)
1	17.88	60
2	19.37	65
3	20.86	70
4	22.35	75
5	23.84	80
6	25.33	85

modulus, and Poisson’s ratio of sandstone obtained from the short-term experiments were 29.8 MPa, 8.4 GPa and 0.29, on average, respectively (Wang et al. 2016). The stress levels of multi-step monotonic creep tests were determined by the constant strain rate tests, set at 60%, 65%, 70%, 75%, 80% and 85% of UCS. The stress loading sequences for multi-step monotonic creep tests are listed in Table 1. Two main stress levels (high stress level, 75.6% of USC; and low stress level, 60% of USC) in the alternating creep tests were confirmed by the multi-step monotonic creep tests to ensure the non-failure of the sample within the test. Besides, the time held at each stage for multi-step monotonic and alternating creep tests was 12 hours. Stress loading sequences for multi-step monotonic creep tests are listed in Table 1 and a schematic diagram of the alternating cyclic creep tests is shown in Fig. 4. Alternating cyclic creep tests were carried out under alternating high and low stress levels. The loading stress is completely removed at the end of stage 6 and kept for 12 hours, and the applied stress level at stage 1 is the same as that at stage 8. Correspondingly, all loading stages are divided into two periods (period I and period II here) by the stage of complete unloading stress, as shown in Fig. 4. Purpose of the stress loading path during period I is to study the influence of alternating high and low stresses on the creep properties of sandstone by comparisons between these two alternating cyclic creep tests. Period II aims to investigate the effects of the stress loading history on the creep property by comparing the creep strain of pre-unloading with that of post-unloading.

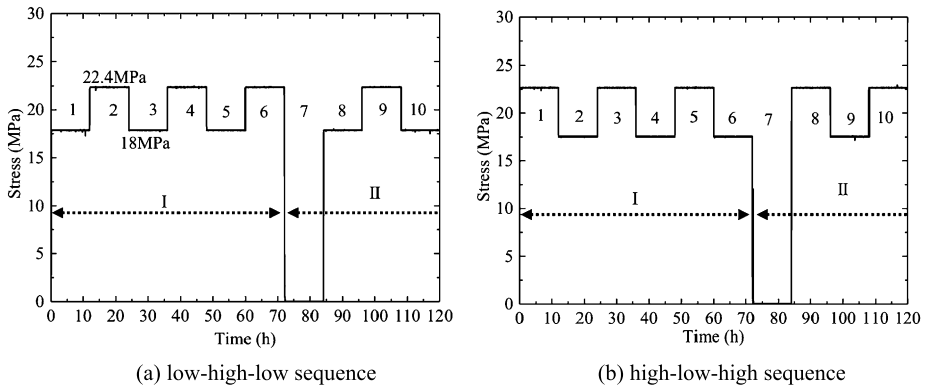


**Fig. 4** Schematic diagram of the alternating cyclic creep tests

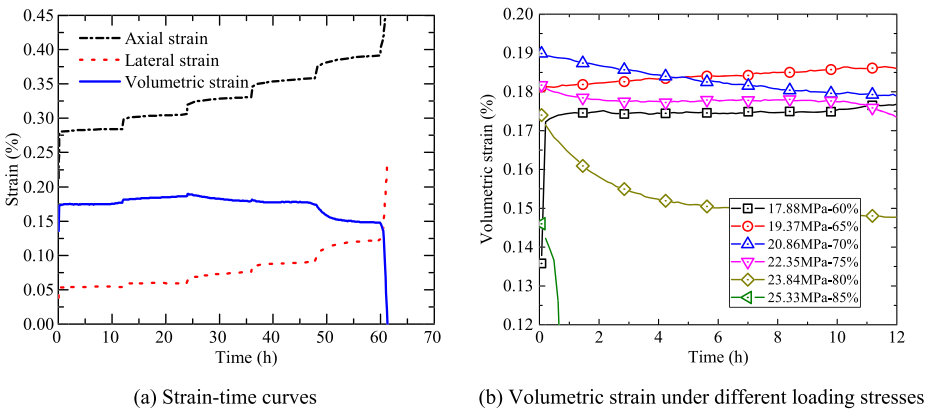


**Fig. 5** Strain-time curves under multi-step monotonic creep tests; note that the volumetric strain was calculated by the axial strain and the lateral strain

### 3 Results

#### 3.1 Uniaxial multi-step monotonic creep tests

To confirm the maximum loading stress and the minimum loading stress in the alternating cyclic creep tests, uniaxial multi-step monotonic creep tests were performed on the sandstone. From the strain-time curve obtained in the multi-step monotonic creep tests (Fig. 5a), the volumetric strain is plotted by loading stress levels as shown in Fig. 5b. Figure 5b shows that the volumetric strain gradually increases with time at the first two stages, at loading stresses of 60% UCS and 65% UCS. But when the loading stress is up to 70% UCS, the volumetric strain starts to decrease. In order to obtain the remarkable creep behavior of rock and meanwhile make sure that the sample wouldn't fail within the alternating cyclic creep tests, the maximum stress was set to 75.6% UCS and the minimum stress to 60% UCS.

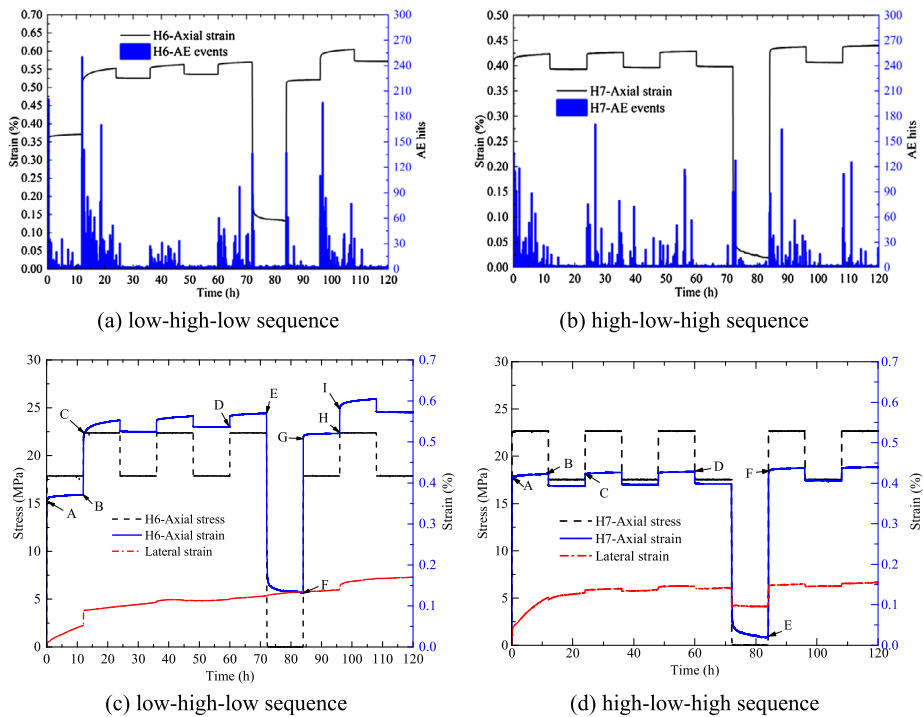


**Fig. 6** Stress, strain and AE hits versus time curves

### 3.2 Alternating cyclic creep tests

As stated above, stresses of 18 MPa (60% stress level) and 22.4 MPa (75.6% stress level) were chosen to perform alternating cyclic loading and unloading creep tests on sandstone to study the effect of alternating cyclic creep tests on the creep properties of sandstone and the influence of loading history on the creep behavior of sandstone. The axial strain, lateral strain and AE hits (or events) curves of sandstone specimens in the alternating cyclic creep tests are shown in Fig. 6. Figure 6a and Fig. 6b show that the clusters of AE hits mainly occur at the high stress stage. The detailed analysis about the AE hits at different stages will be discussed in the next section. From Fig. 6c and Fig. 6d, it can be seen that different high and low stress histories have a great influence on the axial strain and lateral strain, especially the lateral strain.

Figure 6c and Fig. 6d show axial strain and lateral strain at different cyclic loading paths. There are some important points labeled with the letters A, B, C, D, etc., in axial strain-time curves. As shown in Fig. 6c, a large deformation occurs from point B to point C. It can be calculated from Fig. 6c that there is a larger increase (0.144%) in the axial strain from point B to C compared with that from point H to I. As indicated from the axial strain-time curve of the LHL stress sequence, when the loading stress is removed at the end of period I, shown in Fig. 4a, part of axial strain recovers and a residual strain of 0.133% remains at the end of this stage. The axial strain switches immediately up to 0.513%, point G, in Fig. 6c, when the axial stress is reloaded to the stress of 18 MPa at the eighth stage within period II in Fig. 4a. If the strain value at the point G minus the residual strain and the point F in Fig. 6c, the increment strain under loading stress of 18 MPa could be obtained, 0.38%.



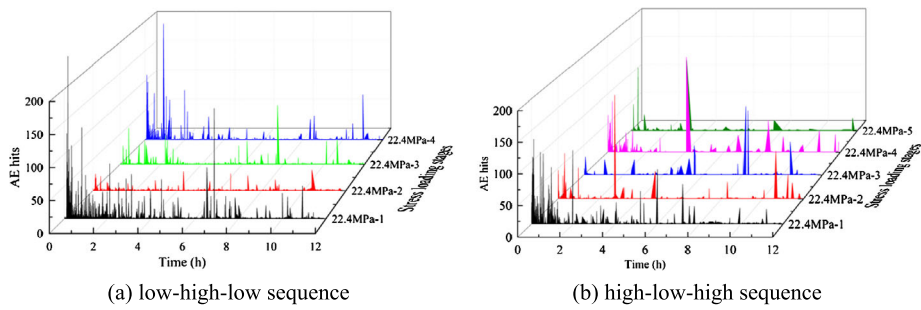


**Fig. 7** AE hits plotted against time at different stages under high loading stress

The strain-time curve of the HLH stress sequence shows that the primary creep strain value (also the end of elastic strain; we assume that the total strain contains elastic strain and creep strain) at the high stress stage within period I starts from the final strain value of the previous high stress stage. For example, the primary creep strain at stage 3, point C, starts from the strain value at point B. When the loading stress is removed, the recovered strain of the HLH stress sequence is much larger than that in H6.

As for the lateral strain-time curves shown in Fig. 6c and Fig. 6d, the lateral strain variation along axial stress is not so much as the corresponding axial strain. But the lateral strain at the first stage for both of loading paths increase sharply, no matter that the loading stress is low or high. In contrast to the variation of axial strain along loading stresses, the lateral strain changes slightly, especially for the stress unloaded from high stress level to low level. Furthermore, when the loading stress is removed, the residual strain in lateral direction is still kept much in the percent of total lateral strain under the maximum loading stress.

### 3.3 Evolution of acoustic emission events at different stages

Compaction, propagation and coalescence of pre-existing cracks, and initiation of new cracks are all accompanied with the release of deformation energy. Normally, the number of AE hits is used to describe the evolution of cracks inside the sample (Eberhardt et al. 1999; Nicksiar and Martin 2012; Shah and Labuz 1995; Xue et al. 2014). In this study, we monitor the compaction of pre-existing cracks and the initiation of new damage cracks by the number of AE hits. The numbers of AE hits (or events) are plotted with time in Fig. 7, separated by the loading stages under high loading stress from the curves of AE hits in Fig. 6.

As shown in Fig. 6a, AE hits were captured mainly at all high stress loading stages of the LHL stress sequence. For all stages having lots of AE hits, we find that the number decreases gradually within every stage. The decrease of AE hits within the stage shows that the specimen gradually stabilizes. It has a common characteristic for both stress sequences that the number of AE hits appearing at the first high stress stage is much higher than that at the others. Therefore, the number of damage appearing at second stage in the LHL sequence is higher than that at first stage in the HLH sequence. As for the HLH stress sequence, the number of AE hits at third stage is higher than that at fifth stage, while it is quite interesting that the number of AE hits at sixth stage for the LHL sequence is higher than that at fourth stage. Besides, the number of AE hits at the stage of stress removed for the HLH stress sequence is higher than that at the corresponding stage for the LHL stress sequence.



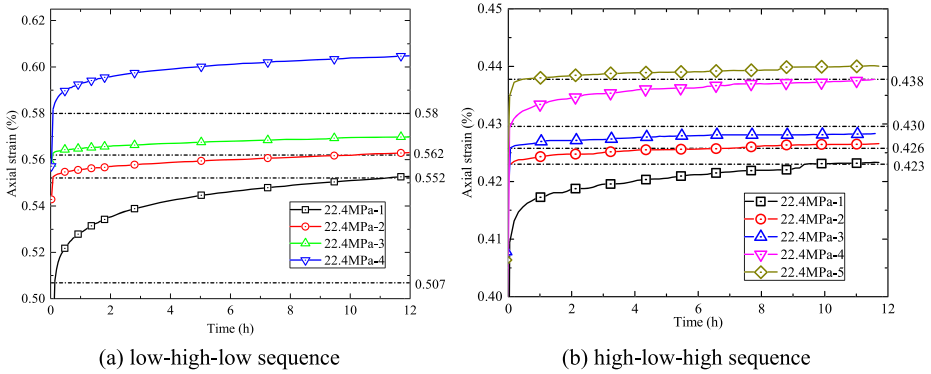


**Fig. 8** Axial strain against time curves divided by loading stages at high loading stress level

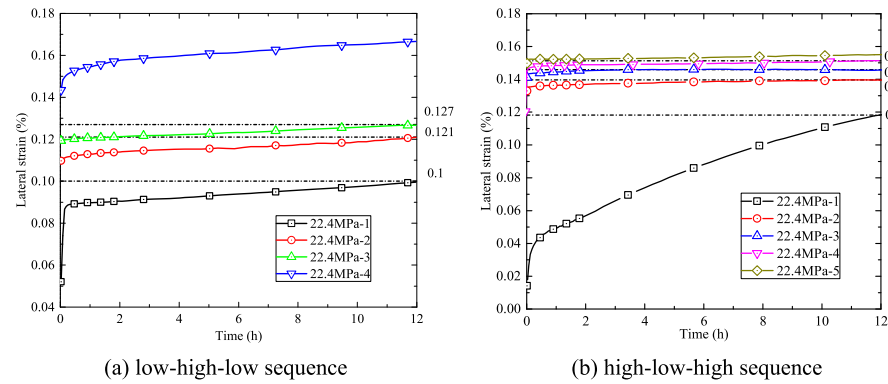


**Fig. 9** Lateral strain-time curves divided by loading stages at high loading stress level

### 3.4 Axial strain under high stress levels

Axial strain curves under high loading stresses were extracted from the loading stages within the same loading paths and plotted in Fig. 8. Figure 8 shows that the axial strain increases with the loading stages even though the loading stress are all same. It should be noted that the primary creep strain of each loading stage within the same period increases almost based on the end of previous creep strain, while the primary creep strain of period II is not based on the end of previous creep strain (at the last high stress stage in the period I). For the LHL stress sequence, the axial strain of fourth high stress stage is affected by the previous low stress stage within period II. As a result, the primary creep strain is higher than the end of creep strain at third stress stage in Fig. 8a.

### 3.5 Lateral strain under the same stress levels

As mentioned before, the lateral strain is more sensitive to the loading stress. Therefore, the lateral strain curves under different loading stages within the same loading paths were also plotted in Fig. 9. Compared with the lateral strain at first loading stages in Fig. 9, it can be found that the strain rate in the LHL sequence should be less than that in the HLH

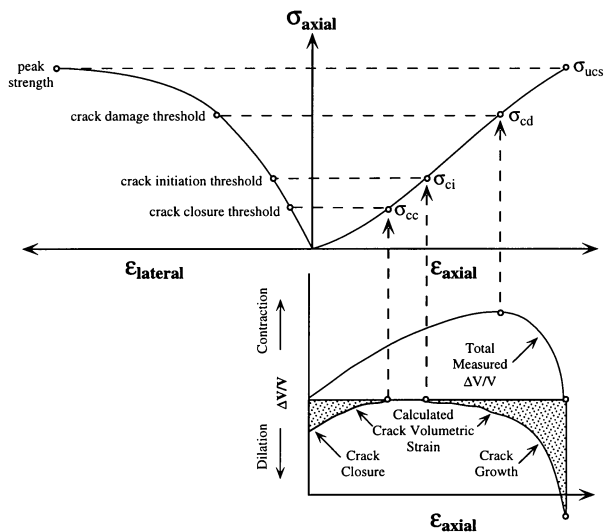
sequence could be got. However, when the loading stress switches to the fourth loading stage, the creep strain is much larger than that at third loading stage. It is a little strange that the difference of lateral strain in the HLH sequence from second to fifth stage is not so much as that in the LHL sequence, especially for the difference between third and fourth stage.

## 4 Discussion

### 4.1 Determination of stress levels in alternating cyclic creep

Heap et al. (2009b) describes that there is a point of the transition of volume from compression to dilation in the differential stress-volumetric strain curve and points out this transition point from the curve of differential stress against volumetric strain in the conventional constant strain rate tests. Zhang et al. (2016a) also recognizes these two phases (a volumetric compaction phase, followed by a dilatancy phase) in the multi-step tri-axial creep tests and the point from the compression to the dilation in the volumetric strain-time curve. Furthermore, some researchers hold the idea that the crack interaction (or unstable crack propagation) threshold is coincident with the point of volumetric strain reversal in uniaxial conditions (Fig. 10) (Diederichs et al. 2004; Eberhardt et al. 1999; Eberhardt et al. 1998). Based on these considerations, we determine the maximum loading stress and the minimum loading stress around this transition point of volume in the alternating cyclic creep tests. And we divided the crack evolution mainly into two parts: the compaction of pre-existing cracks and the initiation of new damage cracks in the crack evolution of this study. The compaction of pre-existing cracks are mainly induced by the loading stress lower than the crack damage threshold (in Fig. 10, or the stress level of volumetric transition), and the initiation of new cracks are principally caused by the applied stress over the damage threshold (Kobayashi 2017). It needs to be pointed out, as per the data published in Ref. (Zhang et al. 2016a), the stress level at the volumetric transition point obtained from conventional uniaxial compressive strength tests is larger than that from multi-step creep tests since the time-dependent evolution of cracks in the sample could accelerate the failure

**Fig. 10** Stress-strain diagram showing the stages of crack development (Eberhardt et al. 1998)



of samples. As a result, the applied stress inducing the crack initiation in the rock sample becomes smaller.

## 4.2 Analysis of crack evolution

### 4.2.1 Analysis of the number of AE hits

Figure 7 shows that the number of AE hits (or events) at the first stage is higher than that at the other stages. It should be noted that the number of AE hits at the fourth stage has a little increase after the loading stress is removed at the previous stage. Some AE hits were captured during the loading, which means that there are some pre-existing cracks compaction, propagation or some new cracks initiation within the stage (Nicksiar and Martin 2012; Xue et al. 2014). Considering the maximum loading stress over the stress point of damage cracks initiation, we could hold the idea that the compaction of pre-existing cracks and the initiation of new cracks occur at the first stage, and the same things happen at fourth stage. However, we could not confirm which one dominates the whole evolution of cracks in the sample under both loading paths, just considering the number of AE hits. Associated with the variation of strain at the corresponding stages, it could be concluded that the compaction of pre-existing cracks dominates the evolution of cracks at the first stage in the LHL stress sequence, and the initiation of new damage cracks dominates at the fourth stage. As for the HLH stress sequence, at both stages the compaction of pre-existing cracks dominates. Finally, the sample in the HLH sequence behaves more like elasticity with less residual strain when the loading stress is removed, but the sample in the LHL sequence shows more plasticity due to the generation of some new cracks.

Compared the number of AE hits in first high loading stress level in the LHL sequence with that in the HLH sequence, it could be noted that the low loading stress at first stage in the LHL sequence does have some influence on the mechanical behavior of the sample. It accelerates the damage occurring inside the specimen. The mechanical behaviors show that the axial strain at first stage under high loading stress in the LHL sequence is larger and the number of AE hits is much higher than that in the HLH sequence. The low loading stress before the high loading stage induces the subsequent variation of axial strain or the number of AE hits under these two loading paths. The curve of AE hits at the subsequent stages of low loading stress are more stable in the LHL sequence than those in the HLH sequence shown in Fig. 6a and Fig. 6b. And the number of AE hits at the subsequent high loading stages is less in the LHL sequence than that in the HLH sequence.

### 4.2.2 Analysis of axial strain

According to the analysis of viscous and plastic behavior of samples (Yang and Hu 2018; Yang et al. 2015; Zhao et al. 2017a, 2017b), two types of strain, viscous strain and plastic strain can be noted in Fig. 6. Special attention should be paid to the viscous behavior of samples when the loading stress is removed. The larger viscous strain in the HLH sequence illustrates that the inner-structure is more stable in the HLH sequence than that in the LHL sequence. In other words, less new cracks appear in the sample of the HLH sequence compared with that in the LHL sequence. The main reason for different mechanical behaviors under different loading paths is the first low stress stage in the LHL sequence. A lot of cracks have been compacted before the high stress stage initiates. Once the high stress is applied on the sample, it is much easier to induce the damage cracks in the inner-structures. In contrast, all of loading stresses are less than that at the first loading stress stage for the HLH

stress sequence in Fig. 6d. Considering the loading stress kept for 12 hours during the first stress stage, the inner-structure of sample H7 experiences a process of stress balance. Most cracks were compacted during this balanced-inter time, and few new cracks initiate. However, there is no higher loading stress applied on the sample, few new cracks would generate under current the maximum loading stress. As a result, the inner-structure of sample in the HLH sequence behaves more stable than that in the LHL sequence.

Figure 6c shows that there is a plastic strain, 0.133% at the point F, after the loading stress is removed, while Fig. 6d illustrates that less plastic strain was generated under the loading path of the HLH sequence. Normally, the initiation of some damage cracks or unstable cracks growth could result in the plastic strain (Nicksiar and Martin 2012). Therefore, there must be some cracks initiation during the previous loading stages in the sample. Besides, the axial strain increases more from point B to C compared with the increasing value from point H to I. The main reason should be that more cracks start to cluster or be connected (damage cracks), or some new cracks initiate at high loading stress after the stage of low loading stress even though the pre-existing cracks may not be compacted completely at the previous stage of low loading stress. Some pre-existing cracks were compacted during the previous stage of low loading stress, and the inner-structure of the sample becomes stable after the loading stress kept for 12 hours. Once the loading stress increased up to a higher level and the high loading stress is over the stress point of volumetric transition from contraction to dilation, the cracks started to initiate under this high stress level. As a result, the axial strain increased sharply and more AE hits occurred at the first high stress stage for the LHL sequence. However, at the subsequent stages, the increment strain from low loading stages to high loading stages is almost the same, which is almost equal to the decrease strain from high loading stages to low loading stages. Therefore, we could conclude that the variation of strain during this transition of stresses is mainly elastic strain. The elastic characteristics of the sample during the subsequent loadings illustrate that there are still some cracks closed and reopened, even when some new cracks generate.

As shown in Figs. 6c and 6d, the influence of loading history on the mechanical behavior of sandstone can be obviously seen by comparison between the increment strain from point F to point G and the strain at point A, 0.36%. It could be explained that the previous alternating cyclic loadings result in the weakness of the inner-structure of the sample. The stress is reloaded to the same level from F to G, more viscous strain and plastic strain are added into the total strain.

#### 4.2.3 Analysis of lateral strain

Compared with that in the HLH sequence, the inner-structure of sample is not so stable after the stress loadings in period I of the LHL sequence due to the initiation of some new cracks. We should hold the idea that the inner-structure of the sample in the HLH sequence is still very stable and few cracks occurs after the preceding stress loadings. Consequently, the creep strain returns back to the previous stress level and keep stable when the loading stress is reloaded back, after the loading stress is removed.

Compared with the percentage of the axial residual strain in total axial strain, much more proportion of lateral residual strain in the total lateral strain has proved that the lateral strain is more sensitive to the loading stress (Nicksiar and Martin 2012). The maximum stress level was set over the transition point of volume from compaction to dilation. Therefore, the lateral volumetric dilation is much higher than that in axial direction under the maximum loading stress (Brantut et al. 2013; Heap et al. 2009b; Xue et al. 2014). The number of new cracks in lateral direction is much higher than that in axial direction, which means that

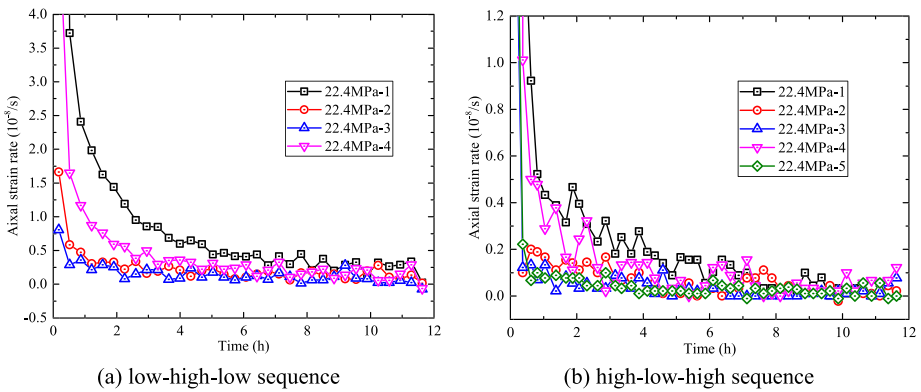


**Fig. 11** Axial strain rate against time at different loading stages under high loading stress

there is no or less of the constraint in the lateral direction all the time during the uniaxial compression tests while the applied stress in the axial direction limited the initiation or the propagation of damaged cracks before the loading stress reaching the point of volumetric transition.

### 4.3 Analysis of crack evolution based on strain rates of separated stages

#### 4.3.1 Axial strain rate

Instant axial creep strain rate against time at different loading stages under high loading stress calculated from Fig. 8 is shown in Fig. 11 to quantify the change trend of strain rates at different loading stages. All of axial strain rate curves firstly decrease sharply and then tend to be stable. And the axial strain rates decrease with the loading stages within the same period, for example the axial strain rate decreases with the stages from the first to the third. However, it should be noted that the curve of strain rate at fourth stage in Fig. 11a lies between the curves at first stage and second stage, which is the result of the loading stress removed before the fourth stage and the inner-structure of the sample partly recovers in elastic and viscous strain.

It should be pointed out that the axial strain rates have some difference under the influence of different loading paths on the mechanical behavior of samples. For instance, the strain rates decrease more sharply at the first stage and the fourth stage for the HLH stress sequence, which means that there are few pre-existing cracks extension and few new cracks initiation. As stated above, there are a few pre-existing cracks extension and lots of new cracks initiation in the LHL stress sequence under high loading stress, so the axial strain rate decreases more slowly, and it needs more time to get into the new stress balance inside the sample experiencing the LHL sequence.

#### 4.3.2 Lateral strain rate

Instant lateral strain rate against time curves at different loading stages under high loading stress were calculated from lateral strain-time curves in Fig. 9 and plotted in Fig. 12. Figure 12 shows that the lateral strain rate has a similar decrease trend with the axial strain rate, decreasing sharply firstly and then leveling off. However, there are still some variation differences between the lateral strain rate and the axial strain rate.

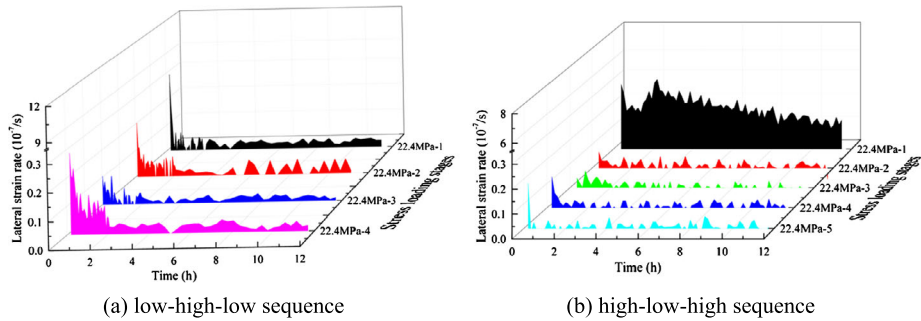


**Fig. 12** Lateral strain rate against time curves at different loading stages under high loading stress

One difference is that the lateral strain rate in the initial time at fourth stage seems higher than that in the other three stages for LHL stress sequence. It can be seen from Fig. 6a that the number of AE hits in fourth stage under high loading stress is not much higher than that in the other three stages, and even less than that in the first high stress stage. The reason is that there are some pre-existing cracks compaction and some new cracks initiation during the first high stress stage. However, the compaction of cracks dominates the increase of AE hits. When the loading stress turns to the fourth stage, the initiation of new cracks dominates the increase of AE hits. Consequently, the lateral strain (in Fig. 8a) and the lateral strain rate at fourth stage is higher than those at the other stages.

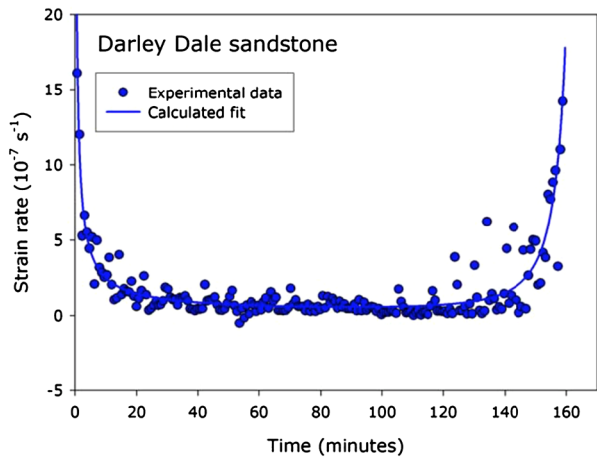
Another difference is that the lateral strain rate at first stage in the HLH stress sequence is higher than that at the other stages, and it decreases slowly within the current loading stage. For the loading path of the HLH stress sequence, the compaction and the initiation of most cracks completed within first high stage. As stated above, the lateral strain is more sensitive to the loading stress. It can be concluded that the performance of lateral strain and lateral strain rate is much more pronounced than that of axial strain and lateral strain rate. Then the “strange” behavior of the lateral strain at first stage in Fig. 9b and the lateral strain rate at first stage in Fig. 12b could be understood easily.

### 4.3.3 Mean strain rate

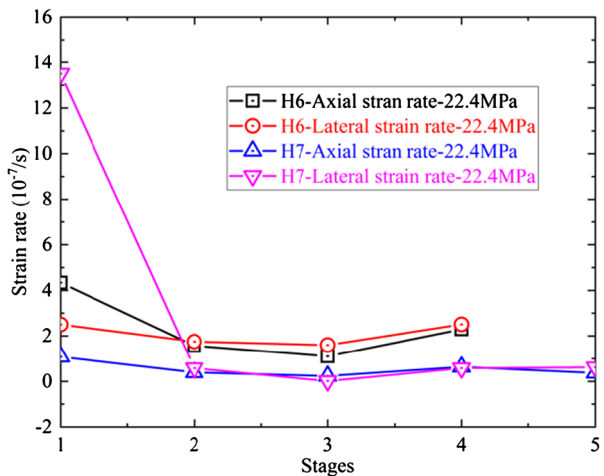
As mentioned in Heap et al. (2009b), in the creep tests the creep strain rate, firstly decrease sharply and then fluctuate within a small range, finally increase till the rock fails (shown in Fig. 13). Our creep strain rate curves at every stage of high loading stress in Fig. 9 have approved the first half of this curve. In order to explore the evolution of creep strain rate under high loading stress, mean creep strain rate was obtained by the average of steady strain rates within the same loading stage in Fig. 11 and Fig. 12, and the curves of mean creep strain rates versus stages are plotted in Fig. 14.

Figure 14 shows that the curve of mean strain rate versus stages behaves a similar trend with the strain rate against time curve in Fig. 11 and Fig. 12. But the decrease trend is not so obvious especially from the first stage to the second since the interior of samples gradually stabilizes after the firstly stage. It should be noted that the dropping trend of lateral strain rate from the first stage to the second for the HLH stress sequence is very evident. As explained before, compared with the variation inside the sample in the LHL sequence, the compaction of pre-existing cracks dominates the process of stress balance inside the sample in the HLH sequence when high loading stress is loaded on it. And the effect of compaction of pre-existing cracks is mainly in the axial direction, which is in agreement with the idea (Chen

**Fig. 13** Strain rate plotted against time curve (Heap et al. 2009b)



**Fig. 14** Mean creep strain rate versus stages under high loading stress



et al. 2018b) that the loading direction plays a role on the crack evolution in the uniaxial condition.

### 5 Applications in underground engineering

As stated above, the loading path plays a significant role in the creep behavior of rock even though the loading stress is less than the peak strength of rock. Clusters of cracks will initiate in the rock if a proper loading path is adopted. In the underground engineering, especially for the mining engineering, sometimes we need to change the condition of field stress by transferring the high loading stress on the surrounding rock to release the stress concentration. There are a lot of engineering applications using this method, such as destress blasting (Konicek 2018; Konicek et al. 2013; Petr et al. 2011), the non-explosive continuous mining technology (Li et al. 2017), and longwall mining method for coal seams (Hamrin and Hustrulid 2001; Islam et al. 2009). Here, we just analyze the method of destress blasting in detail as an example. The main goals of destress blasting are the softening of competent rock



layers, the reduction of strain energy storage, and the release of stress in rock mass, which together contribute to minimizing rockburst occurrence and risk (Konicek 2018). However, the method of destress blasting is still not popular in the mining engineering after almost a century from the first application (Petr et al. 2011). It may be due to the complicated process during the stress transfer, especially for the appearance of damage cracks during mining. Our study provides the evidence that the loading path, even though the maximum loading stress does not reach the peak strength, could affect the mechanical behavior of surrounding rock, which could help to understand the initiation of new damage cracks during the variation of field stress.

## 6 Conclusions

In the present paper we mainly discuss the influence of loading paths and loading histories on the creep characteristics of sandstone under alternating cyclic loading and unloading creep tests to investigate the influence of stress variation induced by mining activities on the creep behavior. The experimental results indicate that the loading paths, low-high-low and high-low-high stress sequences, have great effect on the creep behavior of sandstone. The most obvious characteristics in the strain are the difference of viscous strain and plastic strain during these two loading paths, which is attributed to the difference of new cracks initiation in the sample. It should be noted that the high loading stress and the low loading stress in the alternating cyclic creep tests are set based on the unstable crack threshold, i.e., the volumetric transition from the compaction to the dilation. Based on this unstable crack threshold, it could get more plastic strain on the loading path of low-high-low sequence, compared with that at the high-low-high sequence. It is indicated that more new damage cracks occur in the sample at the low-high-low stress sequence. Besides, the loading history will have a remarkable influence on the viscous strain and the plastic strain in the sample if more damage cracks occur in the samples. While the loading history has a little effect on the inner-structure of the sample on the loading path of high-low-high sequence. It is anticipated that the work could provide some basic understanding about the influence of stress variation on the creep behavior of rock in the underground engineering.

## 7 Acknowledgments

The support provided by Natural Science Foundation of China (Grant Nos. 51974062, 41672301, 51950410595 and 51811530312), National Basic Research Program (973) of China (Grant No. 2017YFC1503100), and Fundamental Research Funds for the Central Universities of China (N180101028) are highly acknowledged. The authors express their gratitude to the suggestion of Dr. Michael Heap from the Laboratoire de Géophysique Expérimentale, Institut de Physique de Globe de Strasbourg, Université de Strasbourg.

**Publisher's Note** Springer Nature remains neutral with regard to jurisdictional claims in published maps and institutional affiliations.

## References

- Armand, G., Noiret, A., Zghondi, J., Seyedi, D.M.: Short- and long-term behaviors of drifts in the Callovo-Oxfordian claystone at the Meuse/Haute-Marne Underground Research Laboratory. *J. Rock Mech. Geotech. Eng.* **5**, 221–230 (2013). <https://doi.org/10.1016/j.jrmge.2013.05.005>

- Atsushi, S., Mitri, H.S.: Numerical investigation into pillar failure induced by time-dependent skin degradation. *J. China Univ. Min. Technol.* **27**, 591–597 (2017). <https://doi.org/10.1016/j.ijmst.2017.05.002>
- Bell, A.F., Naylor, M., Heap, M.J., Main, I.G.: Forecasting volcanic eruptions and other material failure phenomena: an evaluation of the failure forecast method. *Geophys. Res. Lett.* **38**, 165–176 (2011). <https://doi.org/10.1029/2011gl048155>
- Brady, B.H.G., Brown, E.T.: *Rock Mechanics for Underground Mining*. Springer, Berlin (2013)
- Brantut, N., Heap, M.J., Meredith, P.G., Baud, P.: Time-dependent cracking and brittle creep in crustal rocks: a review. *J. Struct. Geol.* **52**, 17–43 (2013). <https://doi.org/10.1016/j.jsg.2013.03.007>
- Brouard, B., Berest, P., de Greef, V., Beraud, J.F., Lheur, C., Hertz, E.: Creep closure rate of a shallow salt cavern at Gellenoncourt, France. *Int. J. Rock Mech. Min. Sci.* **62**, 42–50 (2013). <https://doi.org/10.1016/j.ijrmmms.2012.12.030>
- Cerfontaine, B., Collin, F.: Cyclic and fatigue behaviour of rock materials: review, interpretation and research perspectives. *Rock Mech. Rock Eng.* **51**, 391–414 (2018). <https://doi.org/10.1007/s00603-017-1337-5>
- Challamel, N., Lanos, C., Casandjian, C.: Stability analysis of quasi-brittle materials-creep under multiaxial loading. *Mech. Time-Depend. Mater.* **10**, 35–50 (2006). <https://doi.org/10.1007/s11043-006-9010-5>
- Chen, H., Qi, H., Long, R., Zhang, M.: Research on 10-year tendency of China coal mine accidents and the characteristics of human factors. *Saf. Sci.* **50**, 745–750 (2012). <https://doi.org/10.1016/j.ssci.2011.08.040>
- Chen, C., Xu, T., Heap, M.J., Baud, P.: Influence of unloading and loading stress cycles on the creep behavior of Darley Dale Sandstone. *Int. J. Rock Mech. Min. Sci.* **112**, 55–63 (2018a). <https://doi.org/10.1016/j.ijrmmms.2018.09.002>
- Chen, C.F., Xu, T., Li, S.H.: Microcrack evolution and associated deformation and strength properties of sandstone samples subjected to various strain rates. *Minerals* **8**, 231 (2018b). <https://doi.org/10.3390/Min8060231>
- Diederichs, M.S., Kaiser, P.K., Eberhardt, E.: Damage initiation and propagation in hard rock during tunnelling and the influence of near-face stress rotation. *Int. J. Rock Mech. Min. Sci.* **41**, 785–812 (2004). <https://doi.org/10.1016/j.ijrmmms.2004.02.003>
- Eberhardt, E., Stead, D., Stimpson, B., Read, R.S.: Identifying crack initiation and propagation thresholds in brittle rock. *Can. Geotech. J.* **35**, 222–233 (1998). <https://doi.org/10.1139/t97-091>
- Eberhardt, E., Stead, D., Stimpson, B.: Quantifying progressive pre-peak brittle fracture damage in rock during uniaxial compression. *Int. J. Rock Mech. Min. Sci.* **36**, 361–380 (1999). [https://doi.org/10.1016/S0148-9062\(99\)00019-4](https://doi.org/10.1016/S0148-9062(99)00019-4)
- Eslami, J., Hoxha, D., Grgic, D.: Estimation of the damage of a porous limestone using continuous wave velocity measurements during uniaxial creep tests. *Mech. Mater.* **49**, 51–65 (2012). <https://doi.org/10.1016/j.mechmat.2012.02.003>
- Fabre, G., Pellet, F.: Creep and time-dependent damage in argillaceous rocks. *Int. J. Rock Mech. Min. Sci.* **43**, 950–960 (2006). <https://doi.org/10.1016/j.ijrmmms.2006.02.004>
- Fairhurst, C.: Stress estimation in rock: a brief history and review. *Int. J. Rock Mech. Min. Sci.* **40**, 957–973 (2003). <https://doi.org/10.1016/j.ijrmmms.2003.07.002>
- Hamrin, H., Hustrulid, W.: Underground mining methods and applications. In: Hustrulid, W.A., Hustrulid, W.A., Bullock, R.L., Bullock, R.C. (eds.) *Underground Mining Methods: Engineering Fundamentals and International Case Studies*, Society for Mining, Metallurgy, and Exploration, Colorado, United States, pp. 3–14. (2001)
- Heap, M.J., Baud, P., Meredith, P.G.: Influence of temperature on brittle creep in sandstones. *Geophys. Res. Lett.* **36**, L19305 (2009a). <https://doi.org/10.1029/2009gl039373>
- Heap, M.J., Baud, P., Meredith, P.G., Bell, A.F., Main, I.G.: Time-dependent brittle creep in Darley Dale sandstone. *J. Geophys. Res., Solid Earth* **114**, 2150–2202 (2009b). <https://doi.org/10.1029/2008jb006212>
- Heap, M.J., Baud, P., Meredith, P.G., Vinciguerra, S., Bell, A.F., Main, I.G.: Brittle creep in basalt and its application to time-dependent volcano deformation. *Earth Planet. Sci. Lett.* **307**, 71–82 (2011). <https://doi.org/10.1016/j.epsl.2011.04.035>
- Hu, B., Yang, S-q., Xu, P.: A nonlinear rheological damage model of hard rock. *J. Cent. South Univ. Technol.* **25**, 1665–1677 (2018). <https://doi.org/10.1007/s11771-018-3858-9>
- Islam, M.R., Hayashi, D., Kamruzzaman, A.B.M.: Finite element modeling of stress distributions and problems for multi-slice longwall mining in Bangladesh, with special reference to the Barapukuria coal mine. *Int. J. Coal Geol.* **78**, 91–109 (2009). <https://doi.org/10.1016/j.coal.2008.10.006>
- Jeng, F.S., Weng, M.C., Huang, T.H., Lin, M.L.: Deformational characteristics of weak sandstone and impact to tunnel deformation. *Tunn. Undergr. Space Technol.* **17**, 263–274 (2002). [https://doi.org/10.1016/S0886-7798\(02\)00011-1](https://doi.org/10.1016/S0886-7798(02)00011-1)
- Jeong, S.J., Kim, W.S., Sung, S.J.: Numerical investigation on the flow characteristics and aerodynamic force of the upper airway of patient with obstructive sleep apnea using computational fluid dynamics. *Med. Eng. Phys.* **29**, 637–651 (2007). <https://doi.org/10.1016/j.medengphy.2006.08.017>

- Kaiser, P.K., Cai, M.: Design of rock support system under rockburst condition. *J. Rock Mech. Geotech. Eng.* **4**, 215–227 (2012). <https://doi.org/10.3724/SP.J.1235.2012.00215>
- Kobayashi, M.: Verification of crack opening criterion deduced by newly derived micro-crack evolution equation. *Int. J. Solids Struct.* **106**, 139–151 (2017). <https://doi.org/10.1016/j.ijsolstr.2016.11.025>
- Konicek, P.: Rockburst prevention via distress blasting of competent roof rocks in hard coal longwall mining. *J. S. Afr. Inst. Min. Metall.* **118**, 235–242 (2018). <https://doi.org/10.17159/2411-9717/2018/v118n3a6>
- Konicek, P., Soucek, K., Stas, L., Singh, R.: Long-hole distress blasting for rockburst control during deep underground coal mining. *Int. J. Rock Mech. Min. Sci.* **61**, 141–153 (2013). <https://doi.org/10.1016/j.ijrmms.2013.02.001>
- Kranz, R.L., Harris, W.J., Carter, N.L.: Static fatigue of granite at 200 °C. *Geophys. Res. Lett.* **9**, 1–4 (1982). <https://doi.org/10.1029/GL009i001p00001>
- Li, S., Feng, X.-T., Li, Z., Chen, B., Zhang, C., Zhou, H.: In situ monitoring of rockburst nucleation and evolution in the deeply buried tunnels of Jinping II hydropower station. *Eng. Geol.* **137–138**, 85–96 (2012). <https://doi.org/10.1016/j.enggeo.2012.03.010>
- Li, X.B., Gong, F.Q., Tao, M., Dong, L.J., Du, K., Ma, C.D., Zhou, Z.L., Yin, T.B.: Failure mechanism and coupled static-dynamic loading theory in deep hard rock mining: a review. *J. Rock Mech. Geotech. Eng.* **9**, 767–782 (2017). <https://doi.org/10.1016/j.jrmge.2017.04.004>
- Li, S.H., Zhu, W.C., Niu, L.L., Yu, M., Chen, C.F.: Dynamic characteristics of green sandstone subjected to repetitive impact loading: phenomena and mechanisms. *Rock Mech. Rock Eng.* **51**, 1921–1936 (2018). <https://doi.org/10.1007/s00603-018-1449-6>
- Liu, H.Z., Xie, H.Q., He, J.D., Xiao, M.L., Zhuo, L.: Nonlinear creep damage constitutive model for soft rocks. *Mech. Time-Depend. Mater.* **21**, 73–96 (2017). <https://doi.org/10.1007/s11043-016-9319-7>
- Lyakhovskiy, V., Ben-Zion, Y.: Scaling relations of earthquakes and aseismic deformation in a damage rheology model. *Geophys. J. Int.* **172**, 651–662 (2008). <https://doi.org/10.1111/j.1365-246X.2007.03652.x>
- Mazaira, A., Konicek, P.: Intense rockburst impacts in deep underground construction and their prevention. *Can. Geotech. J.* **52**, 1426–1439 (2015). <https://doi.org/10.1139/cgj-2014-0359>
- Nicksiar, M., Martin, C.D.: Evaluation of methods for determining crack initiation in compression tests on low-porosity rocks. *Rock Mech. Rock Eng.* **45**, 607–617 (2012). <https://doi.org/10.1007/s00603-012-0221-6>
- Niemeijer, A., Spiers, C.J., Bos, B.: Compaction creep of quartz sand at 400–600 degrees C: experimental evidence for dissolution-controlled pressure solution. *Earth Planet. Sci. Lett.* **195**, 261–275 (2002). [https://doi.org/10.1016/S0012-821X\(01\)00593-3](https://doi.org/10.1016/S0012-821X(01)00593-3)
- Petr, K., Mani Ram, S., Hani, M.: Distress blasting in coal mining—state-of-the-art review. *Proc. Eng.* **26**, 179–194 (2011). <https://doi.org/10.1016/j.proeng.2011.11.2157>
- Shah, K.R., Labuz, J.F.: Damage mechanisms in stressed rock from acoustic emission. *J. Geophys. Res., Solid Earth* **100**, 15527–15539 (1995). <https://doi.org/10.1029/95JB01236>
- Sone, H., Zoback, M.D.: Mechanical properties of shale-gas reservoir rocks—part 1: static and dynamic elastic properties and anisotropy. *Geophysics* **78**, D381–D392 (2013a). <https://doi.org/10.1190/geo2013-0050.1>
- Sone, H., Zoback, M.D.: Mechanical properties of shale-gas reservoir rocks — part 2: ductile creep, brittle strength, and their relation to the elastic modulus. *Geophysics* **78**, D393–D402 (2013b). <https://doi.org/10.1190/geo2013-0051.1>
- Sone, H., Zoback, M.D.: Time-dependent deformation of shale gas reservoir rocks and its long-term effect on the in situ state of stress. *Int. J. Rock Mech. Min. Sci.* **69**, 120–132 (2014). <https://doi.org/10.1016/j.ijrmms.2014.04.002>
- Szwedzicki, T.: Rock mass behaviour prior to failure. *Int. J. Rock Mech. Min. Sci.* **40**, 573–584 (2003). [https://doi.org/10.1016/s1365-1609\(03\)00023-6](https://doi.org/10.1016/s1365-1609(03)00023-6)
- Wang, J.B., Liu, X.R., Liu, X.J., Huang, M.: Creep properties and damage model for salt rock under low-frequency cyclic loading. *Geomech. Eng.* **7**, 569–587 (2014). <https://doi.org/10.12989/gae.2014.7.5.569>
- Wang, J.B., Liu, X.R., Song, Z.P., Shao, Z.S.: An improved Maxwell creep model for salt rock. *Geomech. Eng.* **9**, 499–511 (2015). <https://doi.org/10.12989/gae.2015.9.4.499>
- Wang, Q.Y., Zhu, W.C., Xu, T., Niu, L.L., Wei, J.: Numerical simulation of rock creep behavior with a damage-based constitutive law. *Int. J. Geomech.* **17**, 04016044 (2016). [https://doi.org/10.1061/\(ASCE\)GM.1943-5622.0000707](https://doi.org/10.1061/(ASCE)GM.1943-5622.0000707)
- Xu, T., Tang, C.A., Zhao, J., Li, L.C., Heap, M.J.: Modelling the time-dependent rheological behaviour of heterogeneous brittle rocks. *Geophys. J. Int.* **189**, 1781–1796 (2012). <https://doi.org/10.1111/j.1365-246X.2012.05460.x>
- Xu, T., Zhou, G.L., Heap, M.J., Zhu, W.C., Chen, C.F., Baud, P.: The influence of temperature on time-dependent deformation and failure in granite: a mesoscale modeling approach. *Rock Mech. Rock Eng.* **50**, 2345–2364 (2017). <https://doi.org/10.1007/s00603-017-1228-9>

- Xu, T., Zhou, G.L., Heap, M.J., Yang, S.Q., Konietzky, H., Baud, P.: The modeling of time-dependent deformation and fracturing of brittle rocks under varying confining and pore pressures. *Rock Mech. Rock Eng.* **51**, 3241–3263 (2018). <https://doi.org/10.1007/s00603-018-1491-4>
- Xue, L., Qin, S.Q., Sun, Q., Wang, Y.Y., Lee, L.M., Li, W.C.: A study on crack damage stress thresholds of different rock types based on uniaxial compression tests. *Rock Mech. Rock Eng.* **47**, 1183–1195 (2014). <https://doi.org/10.1007/s00603-013-0479-3>
- Yang, J.W., Edwards, R.N.: Predicted groundwater circulation in fractured and unfractured anisotropic porous media driven by nuclear fuel waste heat generation. *Can. J. Earth Sci.* **37**, 1301–1308 (2000). <https://doi.org/10.1139/e00-031>
- Yang, S.Q., Hu, B.: Creep and long-term permeability of a red sandstone subjected to cyclic loading after thermal treatments. *Rock Mech. Rock Eng.* **51**, 2981–3004 (2018). <https://doi.org/10.1007/s00603-018-1528-8>
- Yang, S.Q., Xu, P., Ranjith, P.G., Chen, G.F., Jing, H.W.: Evaluation of creep mechanical behavior of deep-buried marble under triaxial cyclic loading. *Arab. J. Geosci.* **8**, 6567–6582 (2015). <https://doi.org/10.1007/s12517-014-1708-0>
- Zhang, Y., Shao, J., Xu, W., Jia, Y.: Time-dependent behavior of cataclastic rocks in a multi-loading triaxial creep test. *Rock Mech. Rock Eng.* **49**, 3793–3803 (2016a). <https://doi.org/10.1007/s00603-016-0948-6>
- Zhang, Q.Z., Shen, M.R., Ding, W.Q., Jang, H.S., Jang, B.A.: Experimental investigation of long-term characteristics of greenschist. *Geomech. Eng.* **11**, 531–552 (2016b). <https://doi.org/10.12989/gae.2016.11.4.531>
- Zhao, Y.L., Cao, P., Wang, W.J., Wan, W., Liu, Y.K.: Viscoelasto-plastic rheological experiment under circular increment step load and unload and nonlinear creep model of soft rocks. *J. Cent. South Univ. Technol.* **16**, 488–494 (2009). <https://doi.org/10.1007/s11771-009-0082-7>
- Zhao, Y.L., Wang, Y.X., Wang, W.J., Wan, W., Tang, J.Z.: Modeling of non-linear rheological behavior of hard rock using triaxial rheological experiment. *Int. J. Rock Mech. Min. Sci.* **93**, 66–75 (2017a). <https://doi.org/10.1016/j.ijrmms.2017.01.004>
- Zhao, Y.L., Zhang, L.Y., Wang, W.J., Wan, W., Li, S.Q., Ma, W.H., Wang, Y.X.: Creep behavior of intact and cracked limestone under multi-level loading and unloading cycles. *Rock Mech. Rock Eng.* **50**, 1409–1424 (2017b). <https://doi.org/10.1007/s00603-017-1187-1>
- Zhou, H.W., Wang, C.P., Mishnaevsky, L., Duan, Z.Q., Ding, J.Y.: A fractional derivative approach to full creep regions in salt rock. *Mech. Time-Depend. Mater.* **17**, 413–425 (2013). <https://doi.org/10.1007/s11043-012-9193-x>